To appear in *Advanced Robotics*
Vol. 00, No. 00, January 20XX, 1–17

Full paper

Three-dimensional steering for articulated mobile robot with prismatic joints with consideration of hardware limitations

Motoyasu Tanaka[a]*, Mizuki Nakajima[a], Ryo Ariizumi[b], and Kazuo Tanaka[a]

[a]*Department of Mechanical Intelligent Systems Engineering, Graduate School of Information Science and Engineering, The University of Electro-Communication, 1-5-1 Chofugaoka, Chofu, Tokyo, Japan*;
[b]*Department of Mechanical Systems Engineering, Graduate school of Engineering, Nagoya University, Furo-cho, Chikusa-ku, Nagoya, Aichi, Japan*;

(*v1.0 released June 20XX*)

The paper presents a three-dimensional steering method for an articulated mobile robot that contains links, rotational joints, prismatic joints, and active wheels. The robot can change the angles of its links using the rotational joints and vary the lengths of its links using the prismatic joints. The target motion of this robot is represented by a continuous curve and the motions of the joints and the wheels are calculated by fitting the entire robot to this target curve. The forward velocity of the robot's head is adjusted to satisfy the hardware limitations of the robot; e.g., joint angle, joint velocity, and wheel velocity limitations. In addition, a terrain-following method is presented that considers the changes in the lengths of the links. An experimental articulated mobile robot was developed and experiments were carried out to demonstrate the effectiveness of the proposed method.

Keywords: articulated mobile robot; prismatic joint; shift control; constraints;

1. Introduction

Thin serpentine robots that are connected using multiple joints can navigate narrow spaces that humans cannot enter because these robots have thin bodies. Many articulated mobile robots have been developed for inspection of narrow spaces and use in disaster response, e.g., [1, 2]. Articulated mobile robots [1] are composed of links that are serially connected using active joints and a mechanism that generates a propulsive force, such as active wheels [3–6]. These robots can change their entire posture freely by rotating their joints and move using the propulsion mechanism. These robots can not only enter narrow spaces using their thin bodies but can also climb up high steps [5] and stairs [3–5] using their long bodies.

Hirose proposed a locomotion curve for a snake called a *serpenoid curve* in [7] and accomplished undulating locomotion in a snake robot with passive wheeled links that were serially connected using active joints. The snake robot generates its propulsive force via lateral undulation using anisotropic friction caused by the passive wheels. Various control methods have been proposed for this type of snake robot; e.g., biomimetic lateral undulation and lateral rolling [8], control based on a central pattern generator [9], autonomous decentralized control [10], obstacle avoidance [11], and step climbing [12].

The types of snake robots without wheels can move via lateral rolling [13], helical rolling [14, 15], and a locomotion process that involves lifting parts of its body from the ground; examples

*Corresponding author. Email: mtanaka@uec.ac.jp

include traveling wave motion [16], sidewinding [17, 18], pedal wave motion [19], and the crawler gait [20]. In addition, an obstacle-aided locomotion method was proposed in [21].

Robots that have sufficient degrees of freedom to elongate and contract their bodies can move by peristaltic motion in the manner of earthworms. It is easy for these robots to move in narrow spaces because they do not need to undulate laterally to move. These robots move using the expansion and contraction of their bodies combined with changes in the friction between their bodies and the surrounding terrain. Robots of this type have changed the friction by using a one-way clutch wheel in [16, 22, 23], by expansion along the direction of the radius of the robot's body when the link contracts in [24], or by lifting links from the ground in [23, 25, 26].

If the robot has fixed length links, the effect of the link length on its motion is considerable. If the link length is long, the robot can rotate its joints widely, but it is also easy for the joint parts of the robot to make contact with the terrain, causing stacking. In contrast, if the link length is short, it is more difficult for the joint parts to make contact with the terrain, but the robot then has difficulty accessing locations that are high above ground level. In addition, the robot cannot rotate its joints widely because of collisions between the wheels of adjacent links. Therefore, we use an articulated mobile robot with prismatic joints that can vary the length of its links. By changing its link length adaptively, the robot can then avoid unintentional contact with the terrain (thus avoiding stacking), widely rotate its joints, and access high locations.

When controlling a robot that has a prismatic mechanism, predefined peristaltic motion that mimics the motion of worms is most commonly used. In [23], the robot *ACM-S1* was developed; the trunk of this robot's body can vary its length by combining the linear motions of elastic rods, and two-dimensional angleworm and inchworm gaits were achieved using this robot. In [25, 26], three-dimensional gaits were designed using a combination of periodic functions for a prismatic joint and two rotational joints and the designed gaits were demonstrated using the designed robot *slim-slime*. In [24], a peristaltic crawling robot with links that could contract, extent, and bend was developed, and its steering angle was optimized using full-search simulations.

In contrast, a method has been proposed for control of an articulated robot that has extensible and bendable links by representing its body posture as a continuous curve, i.e., a *backbone curve*, in [16]. Using this method, both inextensible traveling wave locomotion and extensible traveling wave locomotion have been accomplished.

If an articulated mobile robot with links that are extensible and bendable moves with extensible motion, then each link moves at a different speed along the length of the entire body, although the head moves at constant speed. The appropriate speed for wheels attached to the body is greatly affected by the link speed. In addition, there is a case where the rotational angle limits vary depending on the lengths of the adjacent links. Therefore, it is necessary to design the robot's motion carefully to satisfy all limitations with respect to the robot hardware, e.g., in terms of its angles and velocities. In particular, if the motion is changed in the situation where an operator operates the robot remotely, it is difficult for the operator to operate the robot manually in a manner that satisfies the hardware limitations.

This paper presents a three-dimensional steering method for an articulated mobile robot that contains links, rotational joints, prismatic joints, and active wheels. In the proposed method, the target command made by an operator is adjusted to ensure that the hardware limitations of the robot are satisfied. In addition, the terrain-following method presented in [5] is upgraded to be applicable to a robot in which the link length changes. The effectiveness of the proposed method is then demonstrated experimentally using the actual robot.

2. Articulated mobile robot with prismatic joints

Figure 1 shows a model of an articulated mobile robot with prismatic joints. This robot has pitch joints, yaw joints, prismatic joints, and wheels. The pitch joint and the yaw joint are alternately but serially connected. The link lengths can be changed using the prismatic joints. Let n be the

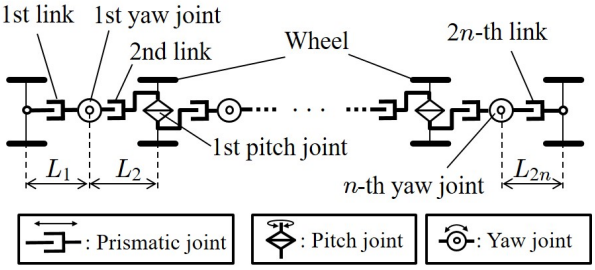

Figure 1. Model of articulated mobile robot with prismatic joints.

number of yaw joints, ϕ_i be the angle of the i-th yaw joint, ψ_i be the i-th pitch joint angle, L_i be the i-th link length, $l_{\max}$ be the maximum link length, and $l_{\min}$ be the minimum link length.

The robot can change the length of its links depending on the surrounding terrain, as shown in Fig. 2. In Fig. 2(a), the long links are 1.5 times longer than the short links and the total length of the robot in the two cases are equal. If the link is shorter, the joint part is less likely to make contact with an obstacle, but the turning radius of the robot is large because the maximum joint angle is small as shown in Fig. 2(a). In contrast, if the link is longer, the turning radius of the robot is small but the joint part makes contact with an obstacle more easily than in the case where the link is short. By changing the length of its links, the robot can both turn with a small radius and avoid collision between the bottom of the joint part and obstacles. Moreover, when the robot raises its head, the load on the pitch joint can be reduced by changing the link length, as shown on the right side of Fig. 2(b). When the link is long, the robot can access locations that are higher above ground level and can cross wider trenches, as shown in Fig. 2(c). Therefore, the appropriate link length is dependent on both the terrain and the target motion of the robot.

3. Three-dimensional steering method

When controlling snake-like robots in three dimensions, a method that uses a continuous curve is commonly used [5, 6, 16, 20, 27–30]. In this method, the robot's target posture is represented by a continuous curve and the joint angles and wheel speeds are then calculated by fitting the entire body of the robot to this continuous curve.

In many works [5, 6, 20, 27–30], the link length of the robot is fixed. In contrast, a method that considers extensible links was proposed in [16]. The representation of the backbone curve when considering extensible links given in [16] is almost the same as that of the method in this paper. However, the method proposed in this paper has the following features that differ from those of [16].

- When implementation on the actual robot is considered, limitations on the operator commands and optimization of the speed are introduced in the proposed method to satisfy the hardware limitations of the actual robot.
- Both the target angles of the joints and the target speeds of the active wheels are calculated because the robot used in this paper has active wheels.
- A terrain-following method in which the robot follows the terrain to relax its joints is incorporated.

Figure 3 shows the control flow diagram for the proposed three-dimensional steering method. First, both the target continuous curve and the robot position on that target curve are updated using the operator's commands while considering the limitations of both the angles of the rotational joints and the speeds of the prismatic joints. Next, the joint angle, the link length, and the wheel velocity are calculated using the target continuous curve in a fitting process. Finally, the robot's forward velocity is adjusted to satisfy any speed limits.

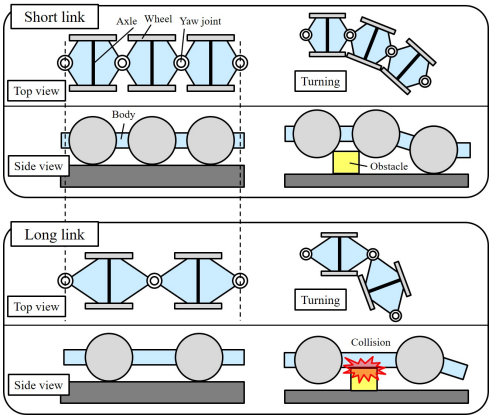

(a) Turning and collision between robot's body and an obstacle

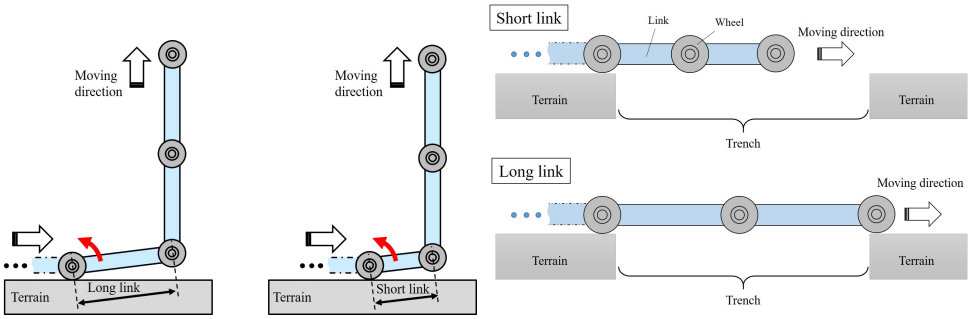

(b) Head raising (side view)

(c) Trench crossing (side view)

Figure 2. Robot motion in the cases where the link lengths are short and long.

As described in [5, 6], a continuous backbone curve is introduced to represent the target robot body posture as

$$\begin{cases} \dfrac{\mathrm{d}\boldsymbol{c}(s)}{\mathrm{d}s} &= \boldsymbol{e}_{\mathrm{r}}(s), \\ \dfrac{\mathrm{d}\boldsymbol{e}_{\mathrm{r}}(s)}{\mathrm{d}s} &= \kappa_{\mathrm{y}}(s)\boldsymbol{e}_{\mathrm{p}}(s) - \kappa_{\mathrm{p}}(s)\boldsymbol{e}_{\mathrm{y}}(s), \\ \dfrac{\mathrm{d}\boldsymbol{e}_{\mathrm{p}}(s)}{\mathrm{d}s} &= -\kappa_{\mathrm{y}}(s)\boldsymbol{e}_{\mathrm{r}}(s), \\ \dfrac{\mathrm{d}\boldsymbol{e}_{\mathrm{y}}(s)}{\mathrm{d}s} &= \kappa_{\mathrm{p}}(s)\boldsymbol{e}_{\mathrm{r}}(s), \end{cases} \tag{1}$$

where s is the length variable along the curve and $\boldsymbol{c} = [x(s), y(s), z(s)]^\top$ is the position vector of the curve. $\boldsymbol{e}_{\mathrm{r}}(s)$ is a tangential unit vector for the curve and $\boldsymbol{e}_{\mathrm{p}}(s)$ and $\boldsymbol{e}_{\mathrm{y}}(s)$ are unit vectors that are oriented along the pitch axis and the yaw axis, respectively. $\kappa_{\mathrm{p}}(s)$ and $\kappa_{\mathrm{y}}(s)$ are the curvatures around the pitch axis and the yaw axis in the curve, respectively. $s = s_{\mathrm{h}}$ is the position of the robot's head on the curve. However, extensible links cannot be represented by (1).

Let $\bar{s}$ be the intervening variable used to fit the robot's body to the continuous curve, let $\bar{s}_0$ be the value of $\bar{s}$ at the head of the robot, let $\bar{s}_i = \bar{s}_0 - il_{\max}$ be the value of $\bar{s}$ for the i-th joint, and let $\bar{s}_{2n} = \bar{s}_0 - 2nl_{\max}$ be the value of $\bar{s}$ for the tail of the robot. $\alpha(\bar{s}) > 0$ is the link stretch rate at $\bar{s}$, and is defined as

$$L_i = \int_{\bar{s}_i}^{\bar{s}_{i-1}} \alpha(\bar{s})\mathrm{d}\bar{s}, \tag{2}$$

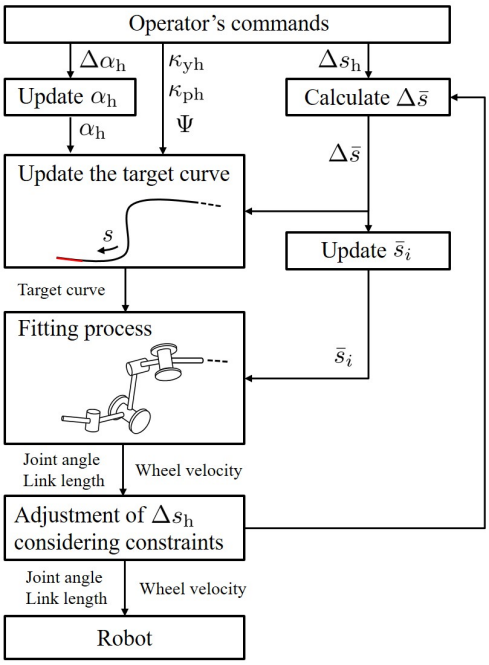

Figure 3. Control flow diagram for the three-dimensional steering method.

where L_i is the length of the i-th link. The link length reaches a maximum when $\alpha(\bar{s}) = 1$, while the link shortens when $\alpha(\bar{s}) < 1$. The relationship between s and $\bar{s}$ can then be represented by

$$\delta s = \alpha(\bar{s})\delta\bar{s}, \tag{3}$$

$$s(\bar{s}) = \int_0^{\bar{s}} \alpha(\tau)\mathrm{d}\tau, \tag{4}$$

where δs and $\delta\bar{s}$ are small-scale variations of s and $\bar{s}$, respectively.

Using (3), the target continuous curve (1) can be represented as follows:

$$\begin{cases} \dfrac{\mathrm{d}\boldsymbol{c}(s(\bar{s}))}{\alpha(\bar{s})\mathrm{d}\bar{s}} = \boldsymbol{e}_\mathrm{r}(s(\bar{s})), \\ \dfrac{\mathrm{d}\boldsymbol{e}_\mathrm{r}(s(\bar{s}))}{\alpha(\bar{s})\mathrm{d}\bar{s}} = \kappa_\mathrm{y}(s(\bar{s}))\boldsymbol{e}_\mathrm{p}(s(\bar{s})) - \kappa_\mathrm{p}(s(\bar{s}))\boldsymbol{e}_\mathrm{y}(s(\bar{s})), \\ \dfrac{\mathrm{d}\boldsymbol{e}_\mathrm{p}(s(\bar{s}))}{\alpha(\bar{s})\mathrm{d}\bar{s}} = -\kappa_\mathrm{y}(s(\bar{s}))\boldsymbol{e}_\mathrm{r}(s(\bar{s})), \\ \dfrac{\mathrm{d}\boldsymbol{e}_\mathrm{y}(s(\bar{s}))}{\alpha(\bar{s})\mathrm{d}\bar{s}} = \kappa_\mathrm{p}(s(\bar{s}))\boldsymbol{e}_\mathrm{r}(s(\bar{s})). \end{cases} \tag{5}$$

Let s_i be the s value for the i-th joint (where $i = 1, 2, \cdots, 2n-1$), and let s_{2n} be the s value for the tail. Figure 4 shows examples of the relationships between a target continuous curve, s, and $\bar{s}$.

3.1 *Updating a target continuous curve*

We extend the curve along the direction of motion in the target continuous curve to let the robot move. Within the short time interval Δt, let Δs_h and $\Delta\bar{s}$ be the variations of s_h and $\bar{s}$, respectively. Assuming that α, κ_y and κ_p are constant at $\bar{s} \in (\bar{s}_0, \bar{s}_0 + \Delta\bar{s}]$, we then set $\alpha(\bar{s}) = \alpha_\mathrm{h}$, $\kappa_\mathrm{y} = \kappa_\mathrm{yh}$ and $\kappa_\mathrm{p} = \kappa_\mathrm{ph}$.

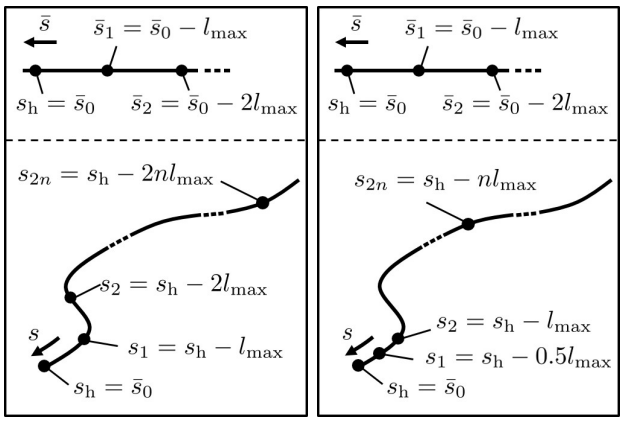

(a) $\alpha(\bar{s}) = 1$, $\bar{s} \in [\bar{s}_{2n}, \bar{s}_0]$ (b) $\alpha(\bar{s}) = 0.5$, $\bar{s} \in [\bar{s}_{2n}, \bar{s}_0]$

Figure 4. Examples of relationships between a target continuous curve, s, and $\bar{s}$.

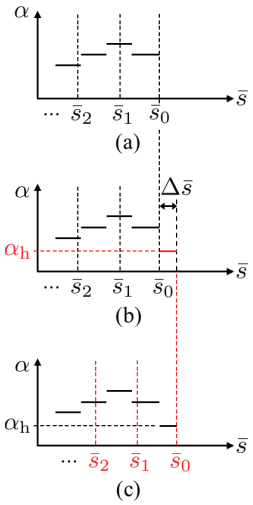

Figure 5. Update process for α. (a) Before updating α and $\bar{s}_i$; (b) after updating α; and (c) after updating α and $\bar{s}_i$.

The operator of the robot enters $\Delta s_{\rm h}$, $\alpha_{\rm h}$, $\kappa_{\rm yh}$ and $\kappa_{\rm ph}$ using an input device such as a gamepad. $\alpha_{\rm h}$ is not provided directly but is designed as

$$\alpha_{\rm h} = \alpha(\bar{s}_0) + \Delta\alpha_{\rm h}, \tag{6}$$

where $\Delta\alpha_{\rm h}$ is the variation of $\alpha_{\rm h}$ that occurs in Δt. Using (6), $\alpha_{\rm h}$ can be set by considering the maximum velocity of the prismatic joints for changing the link length. $\Delta\bar{s}$ can then be obtained as

$$\Delta\bar{s} = \frac{\Delta s_{\rm h}}{\alpha_{\rm h}}. \tag{7}$$

Using $\Delta\bar{s}$ and $\alpha_{\rm h}$, we set $\alpha(\bar{s})$, $\bar{s} \in (\bar{s}_0, \bar{s}_0 + \Delta\bar{s}]$ as shown in Fig. 5(b). By setting $\kappa_{\rm y}$ and $\kappa_{\rm p}$ in a similar manner to α, the target continuous curve is then updated. Finally, all values of $\bar{s}_i$ are updated by adding $\Delta\bar{s}$ as shown in Fig. 5(c) to represent $\bar{s}$ for all joints after Δt. As a result, the position of the robot on the continuous curve has been updated.

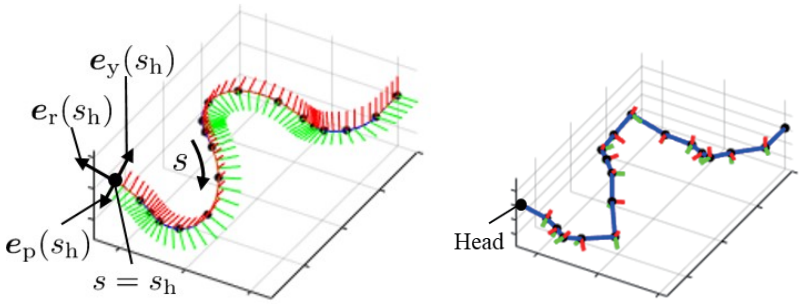

(a) Target continuous backbone curve. Black spheres indicate the positions of each joint. $\boldsymbol{e}_y$(red line) and $\boldsymbol{e}_p$(green line) are drawn at constant intervals of $\bar{s}$.

(b) Robot posture calculated using the shape fitting method. Red lines represent the rotational axis vectors for each joint.

Figure 6. Continuous target curve and robot posture calculated using the fitting method.

In addition, the robot can perform a lateral rolling motion by changing κ_y and κ_p using the method of [5] as follows:

$$\begin{bmatrix} \kappa_y(s(\bar{s})) \\ \kappa_p(s(\bar{s})) \end{bmatrix} = \begin{bmatrix} \cos\Psi & -\sin\Psi \\ \sin\Psi & \cos\Psi \end{bmatrix} \begin{bmatrix} \kappa'_y(s(\bar{s})) \\ \kappa'_p(s(\bar{s})) \end{bmatrix}, \tag{8}$$

where $\kappa'_y(s(\bar{s}))$ and $\kappa'_p(s(\bar{s}))$ represent $\kappa_y(s(\bar{s}))$ and $\kappa_p(s(\bar{s}))$ before the rolling motion, respectively, and Ψ represents the rotational angle around $\boldsymbol{e}_r$.

3.2 *Fitting process*

The angular orientation of the robot can be obtained by fitting the robot's entire body to the target continuous curve. Several suitable fitting methods have been proposed in [6, 27–30]. This work uses a method proposed in [6, 30] because it has low computational costs for calculation of the target angles for the joints. Using this method, the i-th yaw and pitch angles are calculated, respectively, as

$$\phi_i = -\int_{s_{2i}}^{s_{2i-2}} \kappa_y(s)\mathrm{d}s, \tag{9}$$

$$\psi_i = -\int_{s_{2i+1}}^{s_{2i-1}} \kappa_p(s)\mathrm{d}s. \tag{10}$$

By substituting (3) into these equations, ϕ_i and ψ_i can then be represented by

$$\phi_i = -\int_{\bar{s}_{2i}}^{\bar{s}_{2i-2}} \kappa_y(s(\bar{s}))\alpha(\bar{s})\mathrm{d}\bar{s}, \tag{11}$$

$$\psi_i = -\int_{\bar{s}_{2i+1}}^{\bar{s}_{2i-1}} \kappa_p(s(\bar{s}))\alpha(\bar{s})\mathrm{d}\bar{s}. \tag{12}$$

The joint angle based on consideration of the change in the link length can be obtained by (11) and (12). In addition, the i-th link length L_i can be obtained from (2). Figure 6 depicts the posture of a robot obtained using this fitting process.

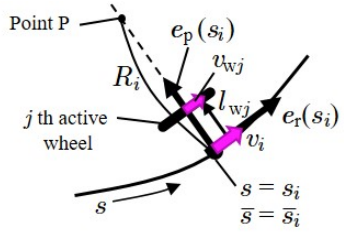

Figure 7. Wheel velocity v_{wj} of j-th active wheel.

Let $v_i = \mathrm{d}s_i/\mathrm{d}t$ be the velocity of the i-th joint on the continuous curve. In [5], $v_1 = v_2 = \cdots = v_{2n-1}$ is satisfied because the link length is fixed. In contrast, not all v_i will have the same value in this case because the link length of the robot used in this work can be varied. Therefore, it is necessary to design the wheel velocity for the robot while considering v_i.

Fig. 7 depicts the wheel velocity relationship on a plane that contains $\boldsymbol{e}_r(s_i)$ and $\boldsymbol{e}_p(s_i)$. Point P represents the center of rotation of the i-th joint on the plane. The distance R_i between the i-th joint and point P can be obtained as

$$R_i = \frac{1}{\kappa_y(s_i)}. \tag{13}$$

Let l_{wj} be the offset distance between $\boldsymbol{c}(s_i)$ and the center of the j-th active wheel. If the wheels on the head and the tail of the robot are passive while the other wheels are active, two active wheels are mounted on the left and right sides of the pitch joint and $j = i-1, i$. From the relationship shown in Fig. 7, the wheel velocity v_{wj} for the j-th active wheel can be obtained as follows.

$$v_{wj} = \begin{cases} \dfrac{(R_i - l_{wj})}{R_i} v_i, & \text{if} \quad \kappa_y(s_i) \neq 0, \\ v_i, & \text{if} \quad \kappa_y(s_i) = 0. \end{cases} \tag{14}$$

3.3 *Introducing limitations*

In the case where the proposed steering method is implemented in the actual robot, it is necessary to move the robot while also satisfying the hardware limitations, including the joint angles, the angular velocities of the joints, the link lengths, the velocities when changing the link lengths, and the wheel velocities.

By limiting the operator commands, we can satisfy the limitations that are not time-dependent, e.g., the joint angles, the link lengths, and the conditions that combine these parameters. Therefore, α_h, κ_{yh}, and κ_{py} are limited to ensure that they satisfy the following conditions.

$$\frac{l_{min}}{l_{max}} \leq \alpha_h \leq 1, \tag{15}$$

$$|\kappa_{yh}| \leq \frac{\phi_{max}}{2 l_{max} \alpha_h}, \tag{16}$$

$$|\kappa_{ph}| \leq \frac{\psi_{max}}{2 l_{max} \alpha_h}, \tag{17}$$

where ϕ_{max} and ψ_{max} are the maximum angles of the yaw joint and the pitch joint, respectively.

In contrast, the angular velocities of the joints, the velocities when varying the link length, and the wheel velocities are dependent not only on Δs_h, κ_y, and κ_p but also on the distribution

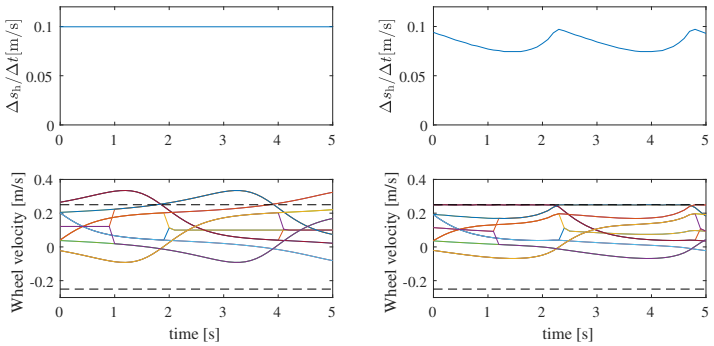

(a) $\Delta s_\mathrm{h}/\Delta t = 0.1$ m/s (b) Adjusting Δs_h using (18)

Figure 8. $\Delta_s\mathrm{h}/\Delta t$ and Wheel velocity with/without adjustment of Δs_h. The broken lines indicate the maximum velocities v_max used in (18).

of the changes in the link lengths of the entire robot. Therefore, we adjust Δs_h appropriately to satisfy these limitations, which are dependent on the velocity. This problem can be formulated as follows using a constrained optimization problem.

$$\underset{\Delta s_\mathrm{h}}{\text{maximize}} \quad \Delta s_\mathrm{h} \tag{18}$$

$$\text{subject to} \quad |\Delta\phi_i| \le \dot{\phi}_\mathrm{max}\Delta t \quad (i = 1, \cdots, n) \tag{19}$$

$$|\Delta\psi_i| \le \dot{\psi}_\mathrm{max}\Delta t \quad (i = 1, \cdots, n-1) \tag{20}$$

$$|\Delta L_i| \le \dot{L}_\mathrm{max}\Delta t \quad (i = 1, \cdots, 2n) \tag{21}$$

$$|v_{\mathrm{w}i}| \le v_\mathrm{max} \quad (i = 1, \cdots, n_\mathrm{w}) \tag{22}$$

where n_w is the number of active wheels, and $\Delta\phi_i$, $\Delta\psi_i$, and ΔL_i are the variations in ϕ_i, ψ_i, and L_i, respectively, caused by Δs_h. $\dot{\phi}_\mathrm{max}$, $\dot{\psi}_\mathrm{max}$, $\dot{L}_\mathrm{max}$, and v_max are the maximum values of $\dot{\phi}_i$, $\dot{\psi}_i$, $\dot{L}_i$, and $v_{\mathrm{w}i}$, respectively. We then obtain the maximum Δs_h numerically using the bisection method for (18). In the bisection method, we set the lower value to 0 and the upper value to the initial Δs_h provided by an operator using a gamepad. The loop is terminated when the difference between Δs_h before and after updating is smaller than a positive minimal value ϵ'.

Figure 8 shows $\Delta s_\mathrm{h}/\Delta t$ and the wheel velocity characteristics when the robot moves forward at $\Delta s_\mathrm{h}/\Delta t = 0.1$ m/s and when $\kappa_\mathrm{yh} = \kappa_\mathrm{ph} = \Delta\alpha_\mathrm{h} = 0$ based on the posture shown in Fig. 6. We set $\epsilon' = 2.5 \times 10^{-5}$ and the number of iterations was 11 in all calculation steps. While the forward velocity of the head was 0.1 m/s, the wheel velocity reached 0.33 m/s when Δs_h was not adjusted because of the effect of changing the link length. In contrast, if Δs_h was adjusted using (18), the wheel velocity could then be fitted under the limit $v_\mathrm{max} = 0.25$ m/s.

3.4 *Terrain-following*

The required terrain-following method has been proposed in [5]. In this method, the robot follows the surrounding terrain by zeroing the torque of the joint; the target continuous curve is then reconstructed using the current posture of the robot and the robot then resumes locomotion from this posture while following the terrain. The robot can follow complex terrain without torque sensors when using the method. In this subsection, we improve the method of [5] to be applicable to an articulated mobile robot with variable link lengths.

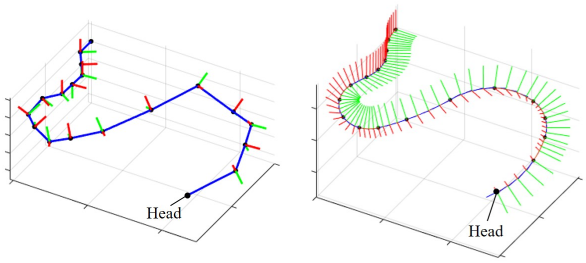

(a) Robot's posture (b) Continuous curve

Figure 9. Reconstruction of target continuous curve using (23) and (24).

In the case where the curvatures of a target continuous curve are calculated from the current joint angle of the robot, the solution is not unique. Therefore, in the same manner as the method in [5], we assume that $\kappa_{\rm y}$ and $\kappa_{\rm p}$ are constants when $(\bar{s}_{2i} < \bar{s} \leq \bar{s}_{2i-2})$ and $(\bar{s}_{2i+1} < \bar{s} \leq \bar{s}_{2i-1})$, respectively. Using this assumption with (11) and (12), $\kappa_{\rm y}$ and $\kappa_{\rm p}$ can then be obtained as

$$\kappa_{\rm y}(s(\bar{s})) = \frac{-\phi_i}{\int_{\bar{s}_{2i}}^{\bar{s}_{2i-2}} \alpha(\bar{s}) {\rm d}\bar{s}}, \quad (\bar{s}_{2i} < \bar{s} \leq \bar{s}_{2i-2}) \tag{23}$$

$$\kappa_{\rm p}(s(\bar{s})) = \frac{-\psi_i}{\int_{\bar{s}_{2i+1}}^{\bar{s}_{2i-1}} \alpha(\bar{s}) {\rm d}\bar{s}}. \quad (\bar{s}_{2i+1} < \bar{s} \leq \bar{s}_{2i-1}) \tag{24}$$

Figure 9 shows an example of the target curve reconstruction process when using (23) and (24). Note that it is possible that the limitation may not be satisfied by the method if the robot has a limitation that combines the joint angle and the link length, such as a limitation that is dependent on the mechanism of the actual robot, as described in the next section.

4. Experiments

We have developed the articulated mobile robot as shown in Fig. 10. This robot has yaw joints, pitch joints, active wheels, and prismatic joint units. The link lengths can be changed using the prismatic joint units. In these units, the rotation of the actuator is transferred to a feed screw through a flat gear; the screw nut then translates along the feed screw and the link length changes. The head and tail do not have active wheels but instead have free wheels. The wheel radius is 0.06 m, the tread width is 0.222 m, $n = 6$, $l_{\rm max} = 0.141$ m, and $l_{\rm min} = 0.093$ m. The total weight and maximum width of the robot are 11.1 kg and 0.245 m, respectively. A Dynamixel XM540-W270-R actuator unit (ROBOTIS Co., Ltd.) is used as the actuator for the rotational joint, while the Dynamixel XM430-W350-R (ROBOTIS Co., Ltd.) is used as the actuator for the wheels and the prismatic joint units.

The power is supplied through the wire shown. The laptop that controls the robot communicates with the robot using the RS485 serial communications interface. The laptop receives the present angle and current of the actuators from the robot. The target angles and velocities of the actuators that are calculated using the laptop are then sent to the robot. In the experiments, the operator sent the commands $\Delta s_{\rm h}$, $\Delta\alpha_{\rm h}$, $\kappa_{\rm yh}$, and $\kappa_{\rm ph}$ to the robot using a gamepad while looking at both the robot and the surrounding terrain using operator's own eyes.

The developed robot cannot rotate its yaw joint when the link length is short because of mechanical interference. Let $\phi_{\rm limit} > 0$ be the limit of $|\phi_i|$ considering mechanical interference.

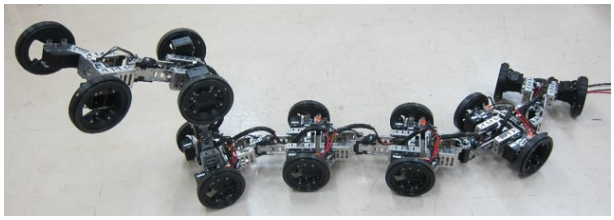

(a) Robot

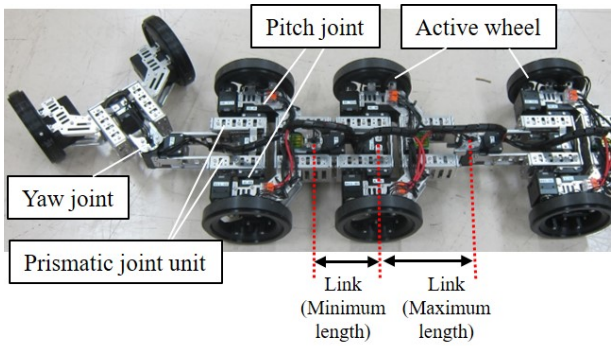

(b) Mechanical structure

Figure 10. Articulated mobile robot with prismatic joints.

Fig. 11 shows the relationship between L_i and ϕ_{limit}. ϕ_{limit} is calculated as

$$\phi_{\mathrm{limit}} = 2\tan^{-1}\left\{\frac{L_i - x_1 + \sqrt{y_1^2 - l_b^2 + (L_i - x_1)^2}}{(y_1 + l_b)}\right\}, \tag{25}$$

where x_1, y_1, and l_b are the geometric parameters as Fig. 11(a), and the maximum value of ϕ_{limit} is limited by the contact between adjacent wheels. We introduce the additional constraint for the operator's input to avoid mechanical interference. First, $\bar{s}$ and α are renewed using Δs_{h} and $\Delta\alpha_{\mathrm{h}}$, and L_1 is calculated by (2). Next, ϕ_{limit} is calculated using L_1 and the relationship in Fig. 11. Considering (11), the maximum value of κ_{y} can be obtained as

$$\kappa_{\mathrm{yU}} = \frac{\phi_{\mathrm{limit}} + \int_{\bar{s}_1}^{\bar{s}_0-\Delta\bar{s}} \kappa_{\mathrm{y}}(s(\bar{s}))\alpha(\bar{s})\mathrm{d}\bar{s}}{\Delta s_{\mathrm{h}}}, \tag{26}$$

$$\kappa_{\mathrm{yL}} = \frac{-\phi_{\mathrm{limit}} + \int_{\bar{s}_1}^{\bar{s}_0-\Delta\bar{s}} \kappa_{\mathrm{y}}(s(\bar{s}))\alpha(\bar{s})\mathrm{d}\bar{s}}{\Delta s_{\mathrm{h}}}, \tag{27}$$

where κ_{yU} and κ_{yL} are the upper and lower limit of κ_{y}, respectively. The mechanical interference can be avoided by limiting the operator input κ_{yh} as $\kappa_{\mathrm{yL}} \leq \kappa_{\mathrm{yh}} \leq \kappa_{\mathrm{yU}}$.

First, we confirmed whether the hardware limitations were satisfied when three-dimensional steering was performed using the proposed method. We used the maximum value depending on the maximum speed of the prismatic joint as $\Delta\alpha_{\mathrm{h}}$. The operator minimized the link length before climbing an obstacle, and maximized the link length after obstacle climbing or before turning. The robot moved forward, turned, and climbed over a step (height of 220 mm, depth of 100 mm) by varying its link length as shown in Fig. 12. At $t > 90$, and $t \simeq 37, 42, 56, 59$, the

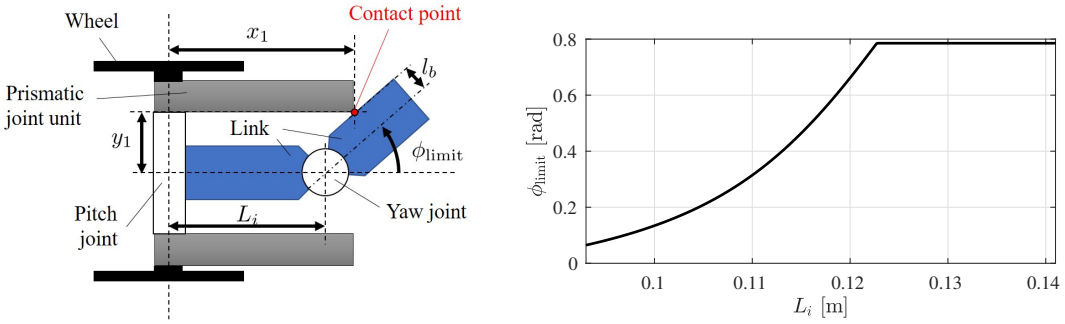

(a) Model (b) Result

Figure 11. The relationship between L_i and ϕ_{limit}.

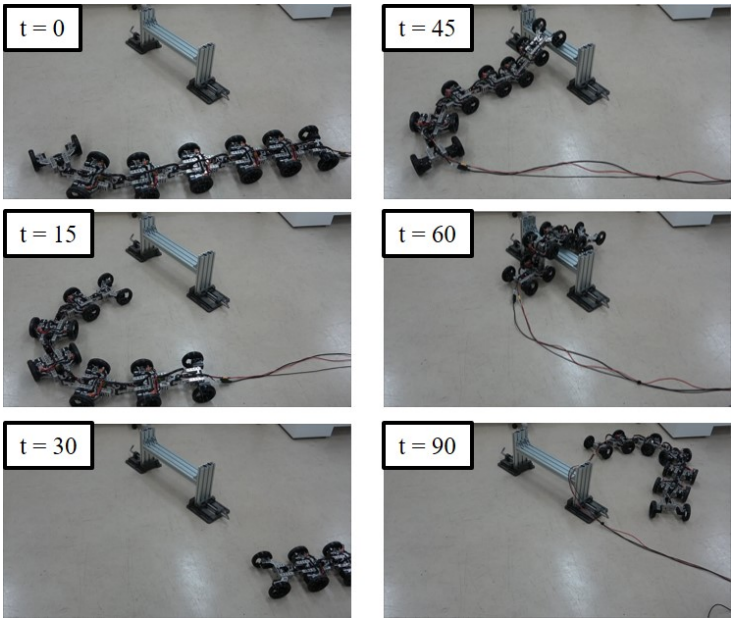

Figure 12. Motion of the robot during three-dimensional steering.

operator provided 0 as the target value Δs_{h} for the robot. At other times, the operator provided the maximum value 0.01. From the results presented in Fig. 13, we find that $\dot{L}_i$, $\dot{\phi}_i$, $\dot{\psi}_i$, and $v_{\text{w}i}$ did not violate the limitations after adjustment of Δs_{h} using (18). The robot's locomotion speed was constrained by the maximum wheel velocity value as shown in Fig. 13(d). Using (15)–(17), the joint angles and link lengths were kept under their limit values, as shown in Fig. 14. In addition, the target angle of the yaw joint was only not zero in the case where the lengths of the links adjacent to the joint were at a maximum following introduction of conditions I and II. As described above, it was confirmed that three-dimensional steering was accomplished while satisfying the hardware limitations when using the proposed method.

The robot performed a step climbing action using to confirm whether it would be necessary to reduce the contact between the joint part of the robot and the surrounding terrain by varying the link length, as indicated in Fig. 2(a). Fig. 15 shows the results. When the link length was at a maximum, the robot became stacked because the body parts in the neighborhood of the yaw joint made contact with the step, as shown in Fig. 15(a). In contrast, when the link length was minimized before the robot climbed the step, the robot was then able to climb the step because the step was in contact with the wheels rather than the joint part, as shown in Fig. 15(b).

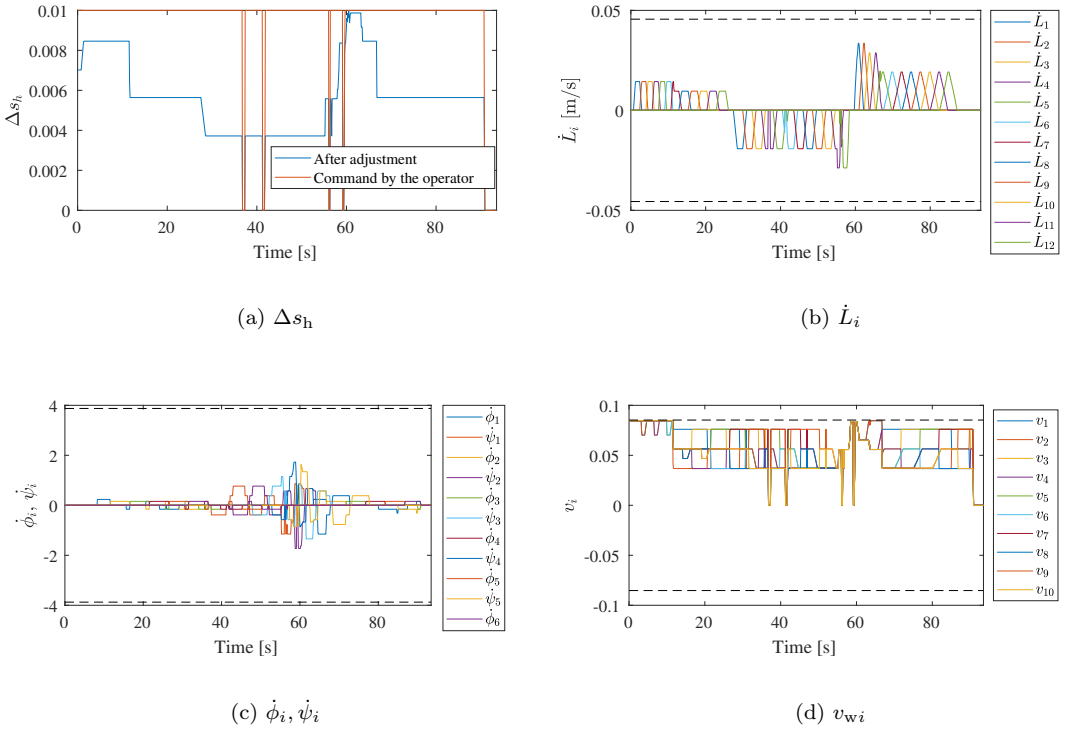

(a) Δs_{h} (b) $\dot{L}_i$

(c) $\dot{\phi}_i, \dot{\psi}_i$ (d) $v_{\mathrm{w}i}$

Figure 13. Δs_{h} and target velocities during three-dimensional steering. The broken lines indicate the maximum and minimum values.

Next, we checked the possibility of executing the head-raising motion shown on the right of Fig. 2(b). Fig. 16 shows the results. The link length reached a minimum before the robot raised its head and the distance between the part lifted by the robot and the pitch joint used to lift the head was shortened. Therefore, the robot can reduce the torque required for the pitch joint when raising its head.

Finally, we tested the terrain-following method. In the experiments, we only applied the terrain-following method to the pitch joints while maintaining the angle of the yaw joint because the yaw joint angle in the actual robot has a limitation that is dependent on the lengths of the links adjacent to the joint and this limitation cannot be satisfied if κ_{y} is updated using the proposed terrain-following method. When the robot climbed the test obstacle, the robot followed the terrain by zeroing the torque of the pitch joint, as shown in Fig. 17(a). We can see that the total amount of current required for the yaw and pitch joints was greatly reduced from the results presented in Fig. 17(b) when using the terrain-following method.

5. Conclusion

This paper proposes a three-dimensional steering method for an articulated mobile robot that contains rotational joints, prismatic joints, and active wheels. The target posture of the robot is represented using an extensible continuous curve and the target robot motion is then calculated by fitting the entire body of the robot to this target continuous curve. Based on consideration of the hardware limitations of the actual robot, the commands that can be given by the operator are limited and the head velocity is adjusted appropriately. While the robot has multiple actuators, the robot can move in a three-dimensional manner using the proposed method while satisfying the hardware limitations. In addition, we improved a previously proposed terrain-following method [5] to be applicable to a robot with variable link lengths. The effectiveness of the proposed method was demonstrated experimentally using the actual designed robot.

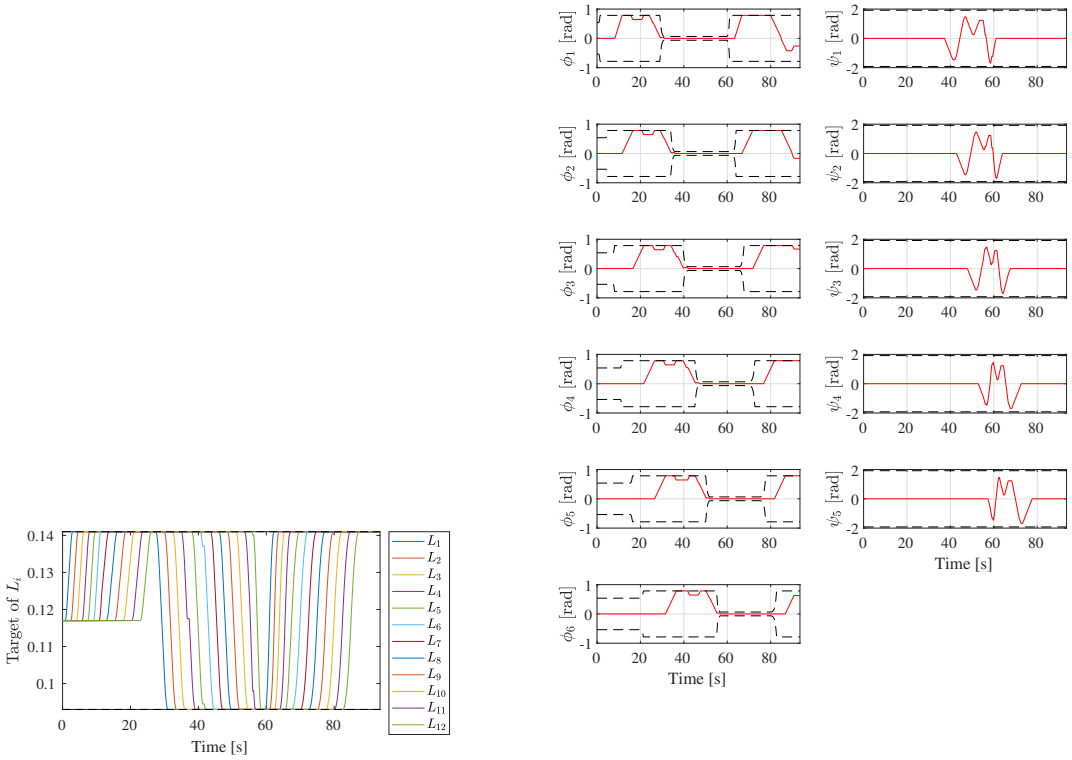

(a) L_i (b) ϕ_i and ψ_i

Figure 14. Target values of L_i, ϕ_i, and ψ_i during three-dimensional steering. The broken lines indicate the maximum and minimum values.

When using the proposed method, the changes in the link length are shifted from the head to tail. In future work, a control method for adaptive adjustment of the link length according to the current situation of the robot will be studied.

Acknowledgements

This work was partially supported by the ImPACT Program of Council for Science, Technology and Innovation (Cabinet Office, Government of Japan); and JSPS KAKENHI under Grant 18K04011. We thank David MacDonald, MSc, from Edanz Group (www.edanzediting.com/ac) for editing a draft of this manuscript .

References

[1] Granosik G. Hypermobile Robots – the Survey. J. of Intelligent and Robotic Systems; 2014; 75-1: 147-169.
[2] Walker ID, Choset H, Chirikjian GS. Snake-Like and Continuum Robots. In: Siciliano B., Khatib O. (eds) Springer Handbook of Robotics; 2016; Springer Handbooks. Springer, Cham.
[3] Borenstein J, Hansen M, Borrell A. The OmniTread OT-4 Serpentine Robot – Design and Performance. J. of Field Robotics; 2007; 24-7:601-621.
[4] Komura H, Yamada H, Hirose S, Endo G, Suzumori K. Development of snake-like robot ACM-R8 with large and mono-tread wheel. Advanced Robotics; 2015; 29-17:1081-1094.

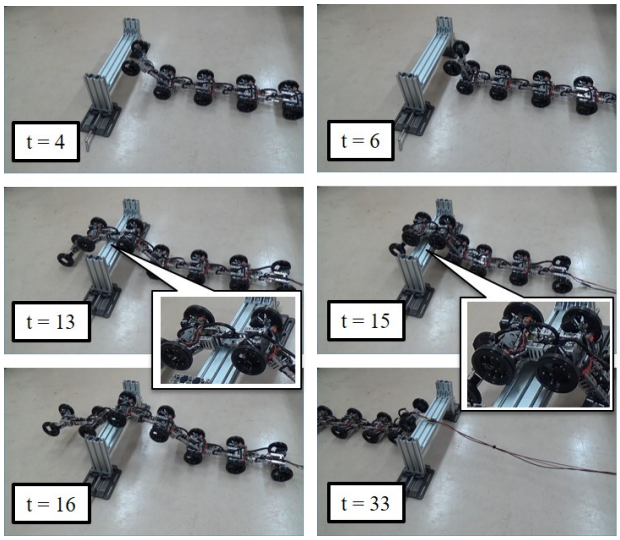

(a) $L_i = l_{\max}$ (b) With change in L_i

Figure 15. Experimental results of step climbing.

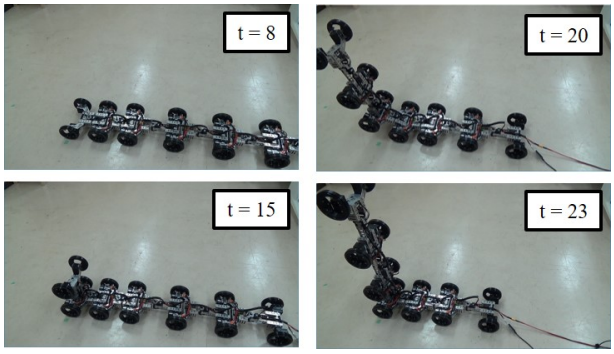

Figure 16. Head-raising motion of the robot.

[5] Tanaka M, Nakajima M, Suzuki Y, Tanaka K. Development and Control of Articulated Mobile Robot for Climbing Steep Stairs. IEEE/ASME Trans. on Mechatronics; 2018; 23-2: 531-541.
[6] Yamada H, Takaoka S, Hirose S. A snake-like robot for real-world inspection applications (the design and control of a practical active cord mechanism. Advanced Robotics; 2013; 27-1:47-60.
[7] Hirose S. Biologically Inspired Robots, Oxford: Oxford University Press; 1993.
[8] Mori M, Hirose S. Three-dimensional serpentine motion and lateral rolling by active cord mechanism ACM-R3. In: Proc. IEEE/RSJ Int. Conf. on Intelligent Robots and Systems; 2002; Lausannne, Switzerland; p829-834.
[9] Crespi A, Ijspeert AJ. Online Optimization of Swimming and Crawling in an Amphibious. IEEE Trans. on Robotics; 2008; 24-1: 75-87.
[10] Sato T, Kano T, Ishiguro A. A decentralized control scheme for an effective coordination of phasic and tonic control in a snake-like robot. BIoinspir. Biommim; 2012; 7-016005; 1-9.
[11] Tanaka M, Kon K, Tanaka K. Range-Sensor-Based Semiautonomous Whole-Body Collision Avoidance of a Snake Robot. IEEE Trans. on Control Systems Technology; 2015; 23-5: 1927-1934.
[12] Tanaka M, Tanaka K. Control of a Snake Robot for Ascending and Descending Steps. IEEE Trans. on Robotics; 2015; 31-2: 511-520.
[13] Mori M, Hirose S. Three-dimensional serpentine motion and lateral rolling by active cord mechanism ACM-R3. In: Proc. IEEE/RSJ Int. Conf. on Intelligent Robots and Systems; Lausanne, Switzerland; 2002; p.829-834.

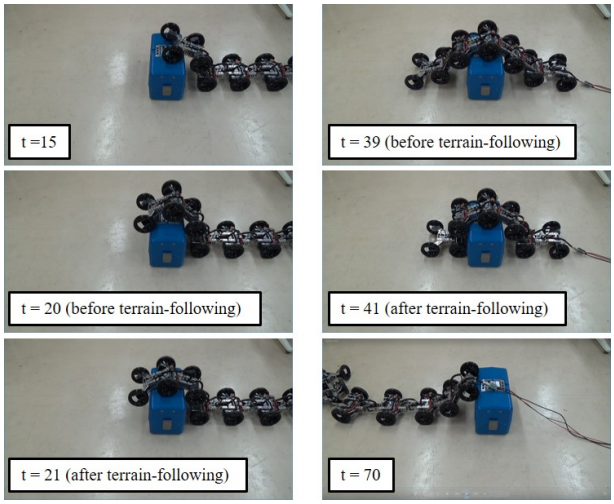

(a) Motion of robot.

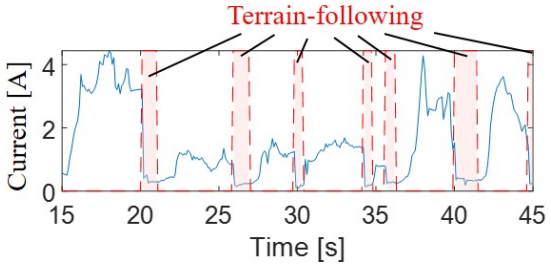

(b) Total current required for angular joints.

Figure 17. Experimental results for terrain-following motion.

[14] Lipkin K, Brown I, Peck A, Choset H, Rembisz J, Gianfortoni P, Naaktgeboren A. Differentiable and piecewise differentiable gaits for snake robots. In: Proc. IEEE/RSJ Int. Conf. on Intelligent Robots and Systems; San Diego, CA, USA; 2007; p.1864-1869.
[15] Baba T, Kameyama Y, Kamegawa T, Gofuku A. A snake robot propelling inside of a pipe with helical rolling motion. In: Proc. SICE Annual Conf 2010; Taipei, Taiwan; 2010; p.2319-2325.
[16] Chirikjian GS, Burdick JW. The Kinematics of Hyper-Redundant Robot Locomotion. IEEE Trans. on Robotics and Automation; 1995; 11-6:781-793.
[17] Burdick JW, Radford J, Chirikjian GS. A 'sidewinding' locomotion gait for hyper-redundant robots. Advanced Robotics; 1995; 9-3: 195-216.
[18] Hatton RL, Choset H. Sidewinding on slopes. In: Proc. IEEE Int. Conf. on Robotics and Automation; Anchorage, AK, USA; 2010; p.691-696.
[19] Yamada H, Hirose S. Steering of Pedal Wave of a Snake-like Robot by Superposition o Curvatures. In: Proc. IEEE/RSJ Int. Conf. on Intelligent Robots and Systems; Taipei, Taiwan; 2010; p.419-424.
[20] Takemori T, Tanaka T, Matsuno F. Gait Design and Experiment for a Snake Robot Designed by Connecting Curve Segments. IEEE Transactions on Robotics; 2018; 34-5:1384-1391.
[21] Transeth AA, Leine RI, Glocker C, Pettersen KY, Liljebäck P. Snake Robot Obstacle-Aided Locomotion: Modeling, Simulations, and Experiments. IEEE Trans. on Robotics; 2008; 24-1: 88-104.
[22] Tang W, Reyes F, Ma S. Study on Rectilinear Locomotion Based on a Snake Robot with Passive Anchor. In: Proc. IEEE/RSJ Int. Conf. on Intelligent Robots and Systems; 2015; Hamburg, Germany. p950-955.
[23] Sugita S, Ogami K, Michele G, Hirose S, Takita K. A Study on Mechanism and Locomotion Strategy for New Snake-Like Robot Active Cord Mechanism–Slime model 1 ACM-S1. J. of Robotics and

Mechatronics; 2008; 20-2: 302-310.
[24] Omori H, Nakamura T, Iwanaga T, Hayakawa T. Development of mobile robots based on peristaltic crawling of an earthworm. In Robotics 2010: Current and Future Challenges Shanghai. InTech, 299-319
[25] Ohno H, Hirose S. Design of Slim Slime Robot and its Gait of Locomotion. In IEEE/RSJ Int. Conf. on Intelligent Robots and Systems; 2001; Maui, Hawaii, USA; p707-715.
[26] Ohno H, Hirose S. A Study of Active Cord Mechanisms -Biomechanical Consideration on its 3D Gaits-. J. of Robotics and Mechatronics; 2003; 15-4: 424-430.
[27] Andersson SB. Discretization of a Continuous Curve. IEEE Trans. on Robotics; 2008; 24-2:456-461.
[28] Hatton RL, Choset H. Generating gaits for snake robots: annealed chain fitting and keyframe wave extraction. Auton. Robot; 2010; 28-3:271-281.
[29] Liljebäck P, Pettersen KY, Stavdahl Ø, Gravdahl JT. A 3D Motion Planning Framework for Snake Robots. In: Proc. IEEE/RSJ Int. Conf. on Intelligent Robots and Systems; 2014; Chicago, IL, USA. p1100-1107.
[30] H. Yamada and S. Hirose, "Study of Active Cord Mechanism –Approximations to Continuous Curves of a Multi-joint Body–," J. of the Robotics Society of Japan, vol.26, no.1, pp. 110-120, 2008 (in Japanese with English summary).